energies

MDPI

Article

From Recycled Polyethylene Terephthalate Waste to High-Value Chemicals and Materials: A Zero-Waste Technology Approach

Maciej Kapkowski [1,*], Sonia Kotowicz [1], Karina Kocot [1], Mateusz Korzec [1], Jerzy Kubacki [2], Maciej Zubko [3,4], Krzysztof Aniołek [3], Urszula Siudyga [5], Tomasz Siudyga [1] and Jaroslaw Polanski [1]

[1] Centre for Materials and Drug Discovery, Institute of Chemistry, University of Silesia, Szkolna 9, 40-006 Katowice, Poland; sonia.kotowicz@us.edu.pl (S.K.); karina.kocot@us.edu.pl (K.K.); mateusz.korzec@us.edu.pl (M.K.); tomasz.siudyga@us.edu.pl (T.S.); jaroslaw.polanski@us.edu.pl (J.P.)
[2] Institute of Physics, University of Silesia, 75 Pułku Piechoty 1A, 41-500 Chorzów, Poland; jerzy.kubacki@us.edu.pl
[3] Institute of Materials Engineering, University of Silesia, 75 Pułku Piechoty 1A, 41-500 Chorzów, Poland; maciej.zubko@us.edu.pl (M.Z.); krzysztof.aniolek@us.edu.pl (K.A.)
[4] Department of Physics, Faculty of Science, University of Hradec Králové, Rokitanského 62, 500 03 Hradec Králové, Czech Republic
[5] Faculty of Health Sciences, Medical University of Silesia in Katowice, Poniatowskiego 15, 40-055 Katowice, Poland; s91726@365.sum.edu.pl
* Correspondence: maciej.kapkowski@us.edu.pl; Tel.: +48-32-349-77-28

Abstract

The presence of PET (polyethylene terephthalate) in the environment is a global problem due to soil and water microplastic contamination. There is a constant demand for new technologies that expand the possibilities of PET disposal or recycling while reducing energy consumption and anthropogenic carbon footprint. In this study, we developed a comprehensive zero-waste management system for PET recycling (rPET) to cyclic ketals and terephthalic acid. The developed method is based on the hydrolysis of rPET flakes in an inert environment with the separation and purification of terephthalic acid and the dehydration of ethylene glycol. For the first time, we present the use of cheap and readily available Cr/SiO_2 and Fe/SiO_2 nanocatalysts for direct acetalization of ethylene glycol without organic co-solvents. The catalysts were characterized by EDXRF, XPS and TEM techniques. The 2,2-dimethyl-1,3-dioxolane (DMD), a product of ethylene glycol's direct acetalization with acetone, was tested as a solvent for polymers with satisfactory results in the solubility of epoxy resins. The addition of unpurified terephthalic acid and residues constituting post-production waste to concrete allows for a reduction in the mass of concrete in the range of 11.3–23.4% and the material modified in this way allows for a reduction in concrete consumption. This rPET waste management methodology is consistent with the assumptions of the circular economy and allows for a significant reduction of anthropogenic CO_2 emissions.

Keywords: rPET; polyethylene terephthalate; terephthalic acid; ethylene glycol recovery; acetalization; nanoparticles; Cr/SiO_2; Fe/SiO_2; concrete modification; circular economy

check for updates

Academic Editor: Peter J. S. Foot

Received: 10 July 2025
Revised: 3 August 2025
Accepted: 13 August 2025
Published: 17 August 2025

Citation: Kapkowski, M.; Kotowicz, S.; Kocot, K.; Korzec, M.; Kubacki, J.; Zubko, M.; Aniołek, K.; Siudyga, U.; Siudyga, T.; Polanski, J. From Recycled Polyethylene Terephthalate Waste to High-Value Chemicals and Materials: A Zero-Waste Technology Approach. *Energies* **2025**, *18*, 4375. https://doi.org/10.3390/en18164375

Copyright: © 2025 by the authors. Licensee MDPI, Basel, Switzerland. This article is an open access article distributed under the terms and conditions of the Creative Commons Attribution (CC BY) license (https://creativecommons.org/licenses/by/4.0/).

1. Introduction

Polyethylene terephthalate (PET), along with polyethylene (PE), polypropylene (PP), polyvinyl chloride (PVC), polyurethane (PUR) and polystyrene (PS), are popular polymers, especially favored in producing food contact packaging, bottles and synthetic fibers. The global PET market is forecasted to grow at a CAGR of 3.2%, from USD 30,577.9 million

in 2025 to approximately USD 41,899.0 million by 2035 [1]. The current problem is the prolonged degradation of PET (over 1000 years), water contamination with micro- and nanoplastics and the release of toxic substances from PET bottles into the environment (phthalates and bisphenol A). The direct impact of releasing harmful substances into water is their accumulation by aquatic organisms [2] and a negative impact on the human endocrine system [3,4]. Moreover, microplastics present in the soil can penetrate plants, accumulate in the roots, negatively affect plant germination and, in low concentrations, penetrate edible parts of plants [5]. As part of the 2030 Agenda, the United Nations has set sustainable development goals, recognizing the threats from irresponsible waste management and trying to direct UN member countries' legislation towards reducing plastic waste and increasing recycling efficiency. Scientists and engineers are also developing co-recycling models. Techno-economic analysis indicates economic and environmental benefits of co-recycling plastics using a method based on chemical recycling with CO_2 or used batteries [6]. Current PET disposal methods consider circular economy trends and focus on recycling. The five primary methods described by Kumar et al. are as follows [7]:

(i) Primary, used exclusively for the disposal of homogeneous post-industrial or pre-consumer waste [8];
(ii) Secondary, based on the disposal of waste on site by washing, sorting, grinding and producing pellets and, in the final phase, by heating, melting and extruding into final products with a lower utility value (photooxidation and mechanical stress of the melted material) [9,10];
(iii) Tertiary, based on chemical recycling using polar solvents and reactions such as glycolysis, methanolysis, hydrolysis, aminolysis and ammonolysis [11–13]. We present a more detailed horizontal comparison of the indicated methods in Table S1, Supplementary Materials;
(iv) Quaternary recycling related to the recovery of energy from plastics through their combustion or pyrolysis [14];
(v) Biodegradation using microorganisms for anaerobic fermentation, aerobic PET composting, or enzymes [15,16].

In a circular economy model, PET is not treated as waste but as a resource that can be used again and again in different forms, as we presented in our previous publication, where functional materials in the aminolysis depolymerization of the waste poly(ethylene terephthalate) were obtained [11,17]. Basing PET disposal methods on well-known, widely inexpensive and readily available catalysts is a key element of the financial profitability of new innovative management and disposal methods.

The application of heterogeneous nanometallic catalysts in environmental protection, especially polymer waste management, is an intensively developing research area [18,19]. The main directions of polymer waste management based on catalysts are energy recovery and fuel production [20–22]. The key to the extraordinary efficiency and activity of nano-catalysts is the large specific surface area and control over the size and shape of nanoparticles [23]. The properties of nanometals and their carriers and the synergy of their mutual interactions are considerable [24]. For example, *Shi* identified four main types of synergistic interactions that can overlap and affect the catalyst activity [25]:

(i) The influence of both catalyst components through their mutual coactivation, consequently leading to an additive effect of enhancing the catalyst activity;
(ii) In multi-stage reactions, catalysis of subsequent reaction stages through interaction (synergy) of two or more catalyst components, consequently leading to increased activity or selectivity of the reaction;

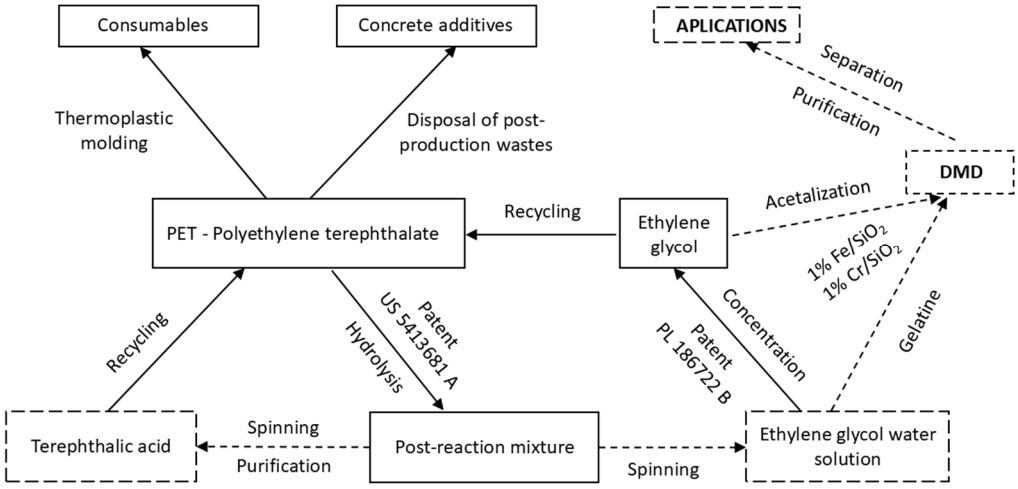
(iii) In reactions conducted in a longer time window, the secondary catalyst component affects the primary one through a protective effect, contributing to limiting its degradation and better stabilization of the catalytic system;
(iv) In red-ox reactions, catalysts can act as storage (e.g., oxygen or hydrogen) or carriers of reagents, supporting their release or binding.

Other significant factors influencing the activity of catalysts are defects in the crystal lattice, the presence of multimetallic systems, electronic modification and the geometry of active centers, particularly active privileged elements [26]. All the above-mentioned phenomena influence the effective operation of the catalyst. The resultants of its activity complement each other, limiting or masking the negative impact of side reactions and reaction conditions. This results in better reaction efficiency and longer catalyst life. The main advantages of heterogeneous nanocatalysts are ease of separation and the possibility of reuse, which aligns with contemporary trends in green chemistry and the circular economy [27]. Recent research also focuses on using photothermal catalysts with grain boundary (GB)-rich CeO_2 for selective recycling of mixed plastic wastes [28].

Methods for synthesizing cyclic ketals in the direct polyol-ketone reaction include three main approaches to their synthesis. Non-catalytic methods include the use of strong organic or inorganic acids. These reactions are supported by the continuous removal of water from the reaction medium. Usually, these systems require organic cosolvents, an inert atmosphere during the reaction and a relatively long reaction time [29]. Catalytic methods involve relatively cheap catalysts from the groups: ion-exchange resins, inorganic solid acids, aluminosilicates or metal oxides with sulfate groups, carbon materials and ionic liquids [30–33]. All the above-mentioned systems are characterized by the presence of active acidic centers (Lewis acids) on the surface, which are necessary for the acetalization reaction. Catalysts based on nanometals or active metal complexes are characterized by high activity parameters (TON) and ensure almost 100% conversion without the need to use special reaction conditions. The literature widely describes the high activity of nanometals or polymetallic systems of Ru, Rh, Ir, Re, Os, In, W, Mo and Sn [34–37] and metal salts or metal complexes of Sc, Ti, Zr, Hf, Y, W, Mo, Co, Ru, Rh, Pd, Pt, Cu, Ni and Ir [29,38,39]. Cyclic acetals and ketals are a group of compounds with wide applications in the agrochemical and petrochemical industries. The most popular applications of simple cyclic acetals include fragrances [38,39], fuel additives [29,40,41], lubricants [42,43], adjuvants [37,44,45], green solvents [46] and factors that increase current density and electrochemical stability in lithium-ion batteries [47–49]. The simplest 1,3-dioxolanes are important in organic synthesis due to their participation in homopolymerization, formaldehyde reactions to produce POM (Polyoxymethylene) and carbonylations [50].

Concrete production is responsible for nearly 8% of global CO_2 emissions, so work is underway to modify its composition and replace some of it with organic and mineral additives to reduce the anthropogenic carbon footprint [51]. Zamora-Castro et al. define that modern sustainable concrete can contain recycled building materials (rubber, plastic, glass and industrial wastes), organic aggregates (bamboo, coconut fiber and nanocellulose) or synthetic fibers (steel, glass, carbon, textile fiber and epoxy resins) [52–56]. The use of these additives not only reduces CO_2 emissions but also improves some properties of concrete, e.g., mechanical properties, anti-corrosive performance or thermal conductivity [51,57,58]. Dawood et al. proved that using PET as a filler in concrete positively affects its strength properties if its content does not exceed 15% [59], and strength standards are the key factor in the concrete constructions (e.g., European standard EN 197-1). At the same time, concrete with a modified composition characterized by reduced mass [55] can be successfully used to produce decorative elements such as flower pots, garden figures or borders. In such applications, aesthetics and durability are more important than structural strength.

In this article, we present the integrated management of rPET waste in a zero-waste technology method (Scheme 1) to reduce energy and raw material consumption. Processing of rPET in the form of flakes involves a stage of neutral hydrolysis of PET [60]. Then, the authors' solution includes separating and purifying terephthalic acid from the solid phase after hydrolysis with the possibility of its reuse in PET production. Ethylene glycol is separated from the liquid phase by dehydration of ethylene glycol using gelatin or by two-stage filtration using polyamide membranes and distillation [61]. In the next step, the ethylene glycol stream is recycled to produce PET or in the reaction with acetone on 1% Fe/SiO_2 or 1% Cr/SiO_2 catalysts, the synthesis and separation of the cyclic ketal 2,2-dimethyl-1,3-dioxolane acting as a valuable adjuvant or fuel additive [29,35,37]. In this study, for the first time, we tested the use of selected 1,3-dioxolane derivatives as potential solvents for polymers from the groups of polyurethanes, polyesters and epoxy resins. The management methodology also includes using unpurified terephthalic acid and post-production waste as an additive to B-20 concrete, modifying the concrete mass (by up to 23%), and is intended to produce garden decorative elements.



Scheme 1. General idea of rPET recycling depending on the chosen path (the dashed lines indicate significant innovation in the rPET recycling process described in this article, the solid lines describe the current known solutions), where the acronym DMD stands for 2,2-dimethyl-1,3-dioxolane.

2. Materials and Methods

2.1. Materials and Preparation of 1% Fe/SiO_2 or 1% Cr/SiO_2

Sol-gel silica was prepared by the Stöber method from 98.0% TEOS—tetraethyl orthosilicate (Acros Organics, Geel, Belgium). Metal precursors were: 99.0% $FeCl_3 \times 6H_2O$ (Warchem, Warszawa, Poland) or 99.0% $CrCl_3 \times 6H_2O$ (Warchem, Warszawa, Poland). Catalysts were prepared by the wet impregnation method. The catalyst powder was reduced in a gaseous hydrogen stream at a temperature of 300 °C. The detailed methodology was described in our earlier publications [29,35,37].

2.2. Methods of Catalyst Characterization

The chemical composition of the catalysts was determined using energy-dispersive X-ray fluorescence (EDXRF) analysis, utilizing an Epsilon 3 spectrometer from Malvern Panalytical, located in Almelo, The Netherlands. This instrument is equipped with a rhodium target X-ray tube, featuring a 50 mm beryllium window and a maximum power output of 9 W. Spectral data were collected using a silicon drift detector (SDD) with an 8 mm beryllium window, providing a resolution of 135 eV at 5.9 keV. The quantitative analysis of the samples was carried out with the Omnian software, which uses a fundamental

parameters method. The measurement conditions were (i) 30 kV in an air atmosphere, using a 100 µm Ag primary beam filter, with a counting time of 120 s, for elements with atomic numbers ranging from 28 to 42 (Ni to Mo) and 72 to 88 (Hf to Ra); (ii) 20 kV in an air atmosphere, using a 200 µm Al primary beam filter, with a counting time of 120 s, for elements with atomic numbers from 24 to 27 (Cr to Co) and 59 to 71 (Pr to Lu); (iii) 12 kV in a helium atmosphere, using a 50 µm Al primary beam filter, with a counting time of 300 s, for elements with atomic numbers from 17 to 23 (Cl to V) and 43 to 56 (Tc to Ba); and (iv) 5 kV in a helium atmosphere, with no filter and a counting time of 300 s, for elements with atomic numbers 11 to 16 (Na to S). The current for each measurement was adjusted to ensure that the deadtime remained below 50%.

The resulting preparations of silica with iron and chromium doping-supported catalysts were examined by X-ray photoemission method XPS with a Prevac/VGScienta photoelectron spectrometer (R3000 electron spectrometer, VG Scienta AB, Uppsala, Sweden and PREVAC sp. z o.o., Rogow, Poland). The survey spectra and core levels of C1s, O1s, Sip2, Fe2p and Cr2p were measured with monochromatic AlK x-ray radiation (h = 1486.8 eV) with pass energy parameters of 200 eV and 100 eV, respectively. All spectra were calibrated to the position of C1s for binding energy E = 285 eV. The shape of the obtained photoemission lines were analyzed using the Multipak program (PHI Multipak SoftwareTM Version 9.6.0.15, Ulvac-phi Inc., Chigasaki, Kanagawa, Japan) from Physical Electronics.

The transmission electron microscopy (TEM) observations were performed using a JEOL (JEOL Ltd., Tokyo, Japan) high-resolution (HRTEM) JEM 3010 microscope working at 300 kV accelerating voltage and equipped with a Gatan (Gatan Inc., Pleasanton, CA, USA) 2k × 2k Orius^{TM} 833SC200D CCD camera and the Elite T Energy Dispersive Spectroscopy (EDS) silicon drift detector (SDD) from AMETEK EDAX (AMETEK Inc., Berwyn, PA, USA). The samples were suspended in isopropanol and the resulting materials were deposited on a Cu grid coated with an amorphous carbon film standardized for TEM observations. Particle size analysis was performed using ImageJ (ver.1.54p—National Institutes of Health, Bethesda, MD, USA), a free of charge computer software.

2.3. Procedure of Synthesis of 1,3-Dioxolane Derivatives

Each time, 20 mg of the catalyst (1.0% Fe/SiO_2 or 1.0% Cr/SiO_2) was introduced into a 20 mL glass test tube equipped with a magnetic stirring bar. The system was closed with PTFE caps (Biotage, Uppsala, Sweden). The following reagents were added, respectively: glycerol 0.37 mL (99.5%, Fisher BioReagents™, Karlsruhe, Germany) or propylene glycol 0.37 mL (99.0% Acros Organics, Geel, Belgium) or ethylene glycol 0.28 mL (99.0% Acros Organics, Geel, Belgium) and acetone 3.73 mL (99.0% Chempur, Piekary Śląskie, Poland). After sealing, the tube was ultrasonically irradiated in an ultrasonic cleaner (Emag Emmi-HC, 40 Hz, Mörfelden-Walldorf, Germany) for 1 min until the sample was uniformly homogenized. The reaction was then carried out on a temperature-controlled magnetic stirrer for 1 h at 55 °C and a rotation speed of 200 rpm. After the reaction was finished, the sample was centrifuged to separate it from the catalyst and the residue. The product was separated and analyzed by NMR technique based on the procedures described in [29].

2.4. Preparation of Standard Curves of Ethylene Glycol Solutions Dehydrated with Gelatine

Two series of ethylene glycol standard solutions were prepared with glycol concentrations of 5, 10, 20, 40, 60, 80 and 99 wt%, respectively. The first series was the reference sample and the second series was dehydrated with gelatin; each time, 0.3 g of granules of gelatin was added without mixing to 9.9 g of previously prepared ethylene glycol solution and dehydrated for 1 h. Then, the solution with swollen gelatin was centrifuged at 5000 rpm for 1–5 min, separating the solid gelatin residue. In the next stage, the dehydrated

solutions were filtered through PTFE syringe membrane filters with a pore size of 5 µm and 0.45 µm. Before the catalyst addition, the filtrate (0.56 mL) was mixed with acetone (7.46 mL) and subjected to ultrasound (1–3 min), resulting in the precipitation of gelatin residues in the form of a white sticky precipitate, which was separated by centrifugation (Figure S1, Supplementary Materials) into a 20 mL glass test tube equipped with the magnetic stirring bar and closing system with PTFE caps (Biotage, Uppsala, Sweden); each time, 4 mL of the dehydrated solution was introduced with the addition of a catalyst: (i) 60 mg 1% Cr/SiO_2; (ii) 60 mg 1% Fe/SiO_2; (iii) 10 mg Amberlyst 15 Hydrogen form (Merck, Darmstadt, Germany); (iv) 60 mg 1% Cr/SiO_2 with 10 mg Amberlyst 15 Hydrogen form (Merck, Darmstadt, Germany); or (v) 60 mg 1% Fe/SiO_2 with 10 mg Amberlyst 15 Hydrogen form (Merck, Darmstadt, Germany). After sealing, the tube was ultrasonically irradiated in an ultrasonic cleaner (Emag Emmi-HC, 40 Hz, Mörfelden-Walldorf, Germany) for 1 min until the sample was uniformly homogenized. The reaction was then carried out on a temperature-controlled magnetic stirrer for 1 h at 55 °C and a rotation speed of 200 rpm. After the reaction was finished, the sample was centrifuged to separate it from the catalyst and the residue was analyzed by NMR technique based on the procedures described in [29].

2.5. Procedure of rPET Hydrolysis and Purification of Terephthalic Acid

The stage of rPET hydrolysis was performed based on previous studies described in the patent [60]. The rPET hydrolysis reaction was carried out in a pressure reactor (Series 4760—Parr Instrument Company, Moline, IL, USA) equipped with a temperature controller with a heating jacket (Series 4838—Parr Instrument Company, Moline, IL, USA). The MR Hei-Tec (Heidolph, Schwabach, Germany) magnetic stirrer was placed under the reactor jacket to ensure continuous mixing of the reactants in the pressure reactor. Into a pressure reactor, the rPET flakes (10 g or 30 g or 40 g) and 40 mL of distilled water were introduced. The reactor was sealed and flushed with nitrogen and then filled with nitrogen to a pressure of 17 bar. Then, the gas supply valve was closed, after which the magnetic stirring and heating jacket connected to the temperature controller were turned on. The rPET hydrolysis was carried out for 2 h from the stabilization of the temperature at 215 °C. After this time, the heating jacket was turned off and left to cool to room temperature, and then the nitrogen was released from the reaction chamber. The solid state residue was filtered under reduced pressure, dried and weighed, and NMR analysis was performed. The results of rPET hydrolysis are summarized in Table 1, while the NMR spectra of liquid residues are presented in Figure S2, Supplementary Materials.

Table 1. The amount of liquid and solid fractions after one rPET hydrolysis cycle.

Entry	rPET Mass [g]	Water [mL]	Solid Residue [g] [a]	Liquid Residue [g]	Ethylene Glycol [%] [b]
1	10	40	8.45	30.00	2.5
2	30	40	28.78	19.20	6.5
3	40	40	47.80	5.31	12.0

[a] The difference in mass balance is due to the drying of the solid residue and the sample cleanup process, as well as minor losses during filtration. A detailed explanation is provided in Scheme S1, Supplementary Materials. [b] Estimated content in the liquid residue determined based on the ^1H NMR spectra shown in Figure S2, Supplementary Materials.

The purification of terephthalic acid from solid residue was carried out using the authors' solution. In the standard procedure, 18 g of solid residue was introduced to a beaker with 400 mL of distilled water, placed on a magnetic stirrer and vigorously mixed. The sodium hydroxide was added in small portions until the solid residue was completely

dissolved and a slightly alkaline pH was reached (checked by indicator paper). Then, 0.3 g of activated carbon was added and stirred for 1 h and the mixture was gravity filtered to separate the activated carbon. Then, concentrated 36% hydrochloric acid (Chempur, Piekary Śląskie, Poland) was added dropwise to the filtrate until an acidic pH was achieved (checked by indicator paper). The precipitate was filtered under reduced pressure and washed with distilled water ca. 300 mL. The product was dried, weighed (final mass—16.13 g) then analyzed via NMR technique (Figure S3, Supplementary Materials). The final purity of terephthalic acid recycled by this methodology was 98.5% (determined by DSC technique) (Figure S4, Supplementary Materials).

2.6. Synthesis of 2,2-Dimethyl-1,3-Dioxolane from Liquid Fraction After rPET Hydrolysis

The liquid parts after neutral pressure hydrolysis of rPET flakes were obtained as in Section 2.5 and were subjected to dehydration with gelatin. In the subsequent variants, the following methodology was used: (i) rPET:H_2O = 10:40 per 21 mL of post-reaction solution, 0.84 g of gelatin was used and dehydrated for 2 h; (ii) rPET:H_2O = 30:40 per 15 mL of post-reaction solution, 0.85 g of gelatin was used and dehydrated for 0.5 h; (iii) rPET:H_2O = 40:40 per 20 mL of post-reaction solution, 0.60 g of gelatin was used and dehydrated for 1.5 h. Then the solution with swollen gelatin was centrifuged at 5000 rpm for 1–5 min, separating the solid gelatin residue. In the next stage, the dehydrated solutions were filtered through PTFE syringe membrane filters with a pore size of 5 µm and 0.45 µm. Before the catalyst addition, the filtrate (0.58–1.0 mL) was mixed with acetone (4.06–14.0 mL) and subjected to ultrasound (1–3 min), resulting in the precipitation of gelatin residues in the form of a white sticky precipitate, which was separated by centrifugation. Into 20 mL glass test tube equipped at magnetic stirring bar and closing system with PTFE caps and (Biotage, Uppsala, Sweden), the dehydrated solutions was introduced with addition of a catalyst: 10–50 mg 1% Cr/SiO_2 or 10–40 mg 1% Fe/SiO_2, both with 10 mg Amberlyst 15 Hydrogen form (Merck, Darmstadt, Germany). After sealing, the tube was ultrasonically irradiated in an ultrasonic cleaner (Emag Emmi-HC, 40 Hz, Mörfelden-Walldorf, Germany) for 1 min until the sample was uniformly homogenized. The reaction was tested under different conditions on a temperature-controlled magnetic stirrer for 30–210 min at 35–60 °C and a rotation speed of 150–400 rpm. After the reaction was finished, the sample was centrifuged to separate it from the catalyst and the residue was analyzed by NMR technique based on the procedures described in [29].

2.7. Procedure of Preparing Concrete Samples with Post-Production Additives

The test samples were prepared using a ready-mix containing B-20 concrete (MTB green line, Poland). The concrete cylinders had a final diameter of 50 mm and a height of 100 mm. Seven samples were prepared with additive contents of 3.5 wt%, and the composition of individual samples is presented in Table 2. The concrete additives consisted of unpurified terephthalic acid from the solid fraction from the rPET hydrolysis described in Section 2.5 and waste from the dehydration of the liquid fraction (gelatin) from the procedure described in Section 2.6. For comparative purposes, the effect of the presence of milled rPET (SM 100 cutting mill Retsch, Haan, Germany) in the form of two fractions with a fineness of 0.25 mm and less than 1 mm on the samples' strength and mass reduction was also checked.

Table 2. Composition of concrete cylinders samples with 3.5 wt.% of selected additives.

Entry	B-20 [g]	Water [g]	rPET [g]	Terephthalic Acid [g]	Gelatine [g]	NH_3/H_2O [mL]
1 ref.	400	62	-	-	-	-
2	388	62	12 *	-	-	-
3	388	70	12 **	-	-	-
4	388	100	-	12	-	-
5	388	100	-	12	-	2.4/50
6	388	85	-	10.8	1.2	2.2/50
7	388	70	6 **	6	-	-

Acronyms: ref.—reference sample; B-20—concrete class B-20; rPET—milled flakes of polyethylene terephthalate; respectively, * fraction 0.25 mm and ** fraction < 1 mm.

2.8. Compressive Strength Tests of Concrete Samples

A static compression test was conducted using the INSTRON 5982 testing machine, computer-controlled by the BLUEHILL 3 software. Cylindrical specimens with a diameter of 50 mm and a height of 100 mm were used for this study. The crosshead speed of the machine during the tests was set at 0.2 mm/min. During the tests, compression curves were recorded in the coordinate system: compressive stress σ—relative strain ε. The compressive strength was determined in this study according to the following relationship:

$$R_c = \frac{F}{A}$$

where R_c—compressive strength [MPa], F_{max}—maximum force [N] and A—cross-sectional area of the sample [mm^2].

2.9. 1,3-Dioxolanes Derivatives Tests in Polymers Solubility

Then, 0.1 g of polymer/foam/glue was weighed into a glass vessel and 1 cm^3 of 1,3-dioxolanes were added, mechanically shaken for 15 s and left at room temperature. Solubility was monitored at 0, 2, 5, 15, 30 and 45 min and at 1, 2, 5, 12, 24 and 48 h. After 24 h, in the case of polyurethane foam, additional 1,3-dioxolanes were added. The low-pressure polyurethane foam contained diphenylmethane diisocyanate, isomers and homologues, chlorinated paraffins and, C14-C17 (Tytan Professional, Wrocław, Poland). The two-component epoxy glue (Plastipox) contained methyl methacrylate, methacrylic acid, cumene hydroperoxide, 4-methylbenzylsulfonyl chloride (K2, Ostrów Wielkopolski, Poland). Polymers (PMMA, PEN, HDPE and PP) were purchased from Merck (Darmstadt, Germany).

3. Results and Discussion

The EDXRF spectrum of 1% Cr/SiO_2 depicted in Figure 1a contains the Si Kα peak at 1.74 keV corresponding to silicon (Si) from the SiO_2 support. The peak at approximately 3.69 keV arises from calcium (Ca Kα), potentially a contaminant or trace element in the sample. The highly intense Cr Kα peak at 5.41 keV and Cr Kβ peak at 5.94 keV confirm the presence of chromium (Cr), which is the primary element of interest. The Fe Kα peak at 6.40 keV suggests the presence of iron (Fe), likely as a trace contaminant. The Zn Kα peak at 8.63 keV shows that there are also trace amounts of zinc (Zn) in the sample. The Rh Kα peak at 20.21 keV and Rh Kβ peak at 22.72 keV originate from the rhodium (Rh) X-ray tube target used in the instrument for excitation. Compton scattering peaks between 15 and 20 keV result from X-ray interactions with the sample. The peaks corresponding to the Ag L lines are observed around 3.00–3.80 keV. These peaks are attributed to the silver primary beam filter used during the experiment and do not indicate the presence of silver

in the sample itself. The most prominent feature in the 1% Fe/SiO_2 spectrum is a peak at 6.40 keV, corresponding to the Fe Kα line (Figure 1b). This confirms the presence of iron in the sample. A smaller peak at 7.06 keV corresponds to the Fe Kβ line, providing further evidence of iron's presence. At the lower end of the energy spectrum, a small peak at 1.74 keV corresponds to the Si Kα line. This peak originates from the silicon dioxide (SiO_2) substrate on which the iron is deposited. The peak observed at 3.69 keV is attributed to the Ca Kα line. The presence of calcium may indicate minor contamination or impurities within the sample or substrate. Peaks at 8.04 keV and 8.63 keV correspond to the Cu Kα and Zn Kα lines, respectively. Detecting copper and zinc suggests possible contamination from environmental exposure or sample-handling equipment. In the inset section of the spectrum, peaks around 3.69 keV appear to correspond to the Ag L lines. However, silver is not present in the sample. These features are attributed to the primary beam filter used in the measurement. At the higher-energy end of the spectrum, peaks at 20.21 keV and 22.72 keV correspond to the Rh Kα and Rh Kβ lines, respectively. Compton scattering peaks accompany these. The results of qualitative and quantitative analysis are summarized in Table 3.

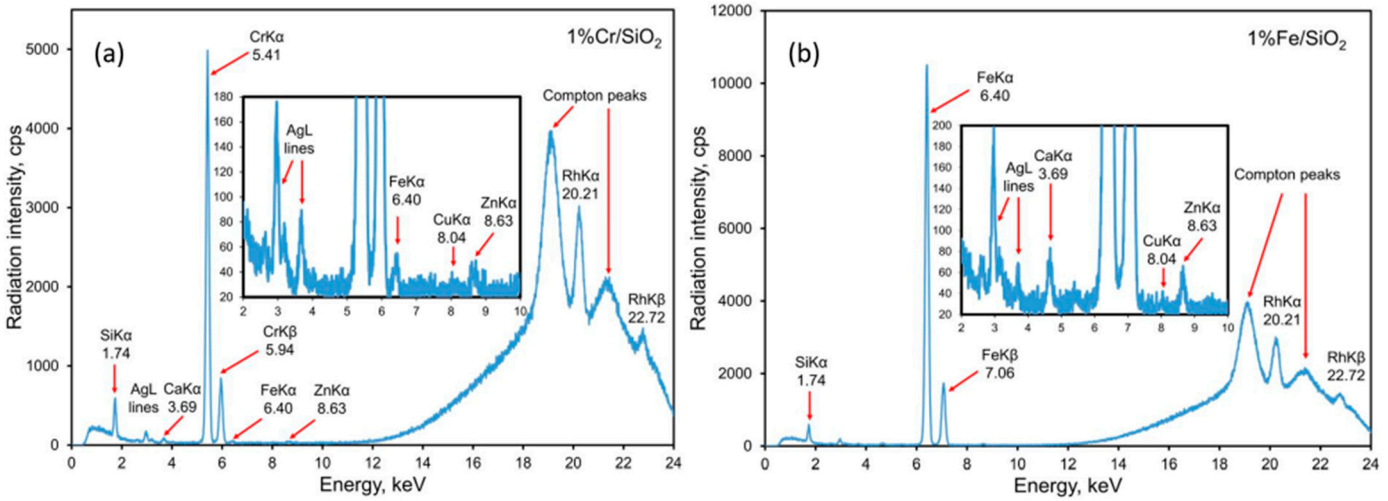


Figure 1. (**a**) Energy-dispersive X-ray fluorescence (EDXRF) spectrum of the 1%Cr/SiO_2 catalyst. The measurement was conducted using a 30 kV voltage in an air atmosphere, with a 100 µm silver primary beam filter and a counting time of 120 s. Characteristic peaks for Si Kα (1.74 keV), Cr Kα (5.41 keV), Cr Kβ (5.94 keV), Fe Kα (6.40 keV) and Zn Kα (8.63 keV) are visible. Rh Kα (20.21 keV) and Rh Kβ (22.72 keV) peaks originate from the Rh target of the X-ray tube. (**b**) X-ray fluorescence (XRF) spectrum of the 1% Fe/SiO_2 sample measured at 30 kV in an air atmosphere using a 100 µm silver (Ag) primary beam filter, with a counting time of 120 s. Characteristic peaks for Si Kα (1.74 keV), Cr Kα (5.41 keV), Cr Kβ (5.94 keV), Fe Kα (6.40 keV) and Zn Kα (8.63 keV) are visible. Rh Kα (20.21 keV) and Rh Kβ (22.72 keV) peaks originate from the Rh target of the X-ray tube.

Table 3. EDXRF qualitative and quantitative analysis of Cr or Fe NPs deposited at sol-gel silica.

Entry	Catalyst	Chemical Element [wt%]					
		Fe	Cr	P	Al	Cl	SiO_2
1	SiO_2	43 *	-	0.087	0.133	15 *	99.434
2	1.0% Fe/SiO_2	0.910	-	917.3 *	-	0.268	98.688
3	1.0% Cr/SiO_2	9.2 *	0.983	878.4 *	0.119	-	98.520

* value in ppm.

In Figure 2, the survey spectra of the studied samples are presented. The photoemission lines consist of several peaks related to the electronic states of Si2p, Si2s, O1s and O KLL as the main components of the studied samples. The small signal of C1s indicates the sound quality of the obtained nanomaterials. In insets 1b and 1c, we show a section of the overview spectrum with markings of the electronic states of Fe2p and Cr2p. Small features on the spectra indicate the successful addition of iron atoms and chromium at a nominal 1% to the SiO_2 base silica.

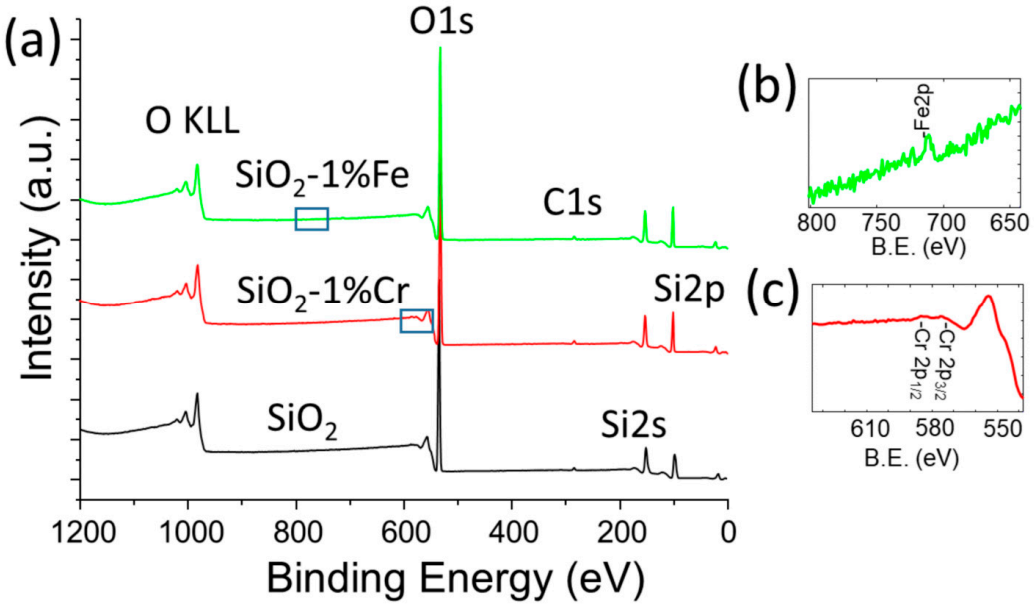


Figure 2. The photoemission survey spectra obtained for source material SiO_2 and containing of 1% nominal of iron and chromium (**a**). Enlarged area of survey spectrum marked by blue rectangles in the range of binding energy related to the position of Fe2p and Cr2p core levels are shown in inset (**b**) and (**c**).

Figure 3 collects the Si2p, C1s and O1s core levels. The position of the C1s and O1s peaks equals 285 eV and 533 eV for all samples. In the case of a silica sample with additive components of iron and chromium, the position of the Si2p peak at 103.6 eV corresponds to the SiO2 function. The Si2p peak is shifted by about 4 eV towards lower energy for the reference sample. It consists of two spin–orbit doublets related to the clean Si and SiO chemical states in the base material before applying the chemical procedure [62]. The Si2p deconvoluted lines are presented in Figure S5 of the Supplementary Materials.

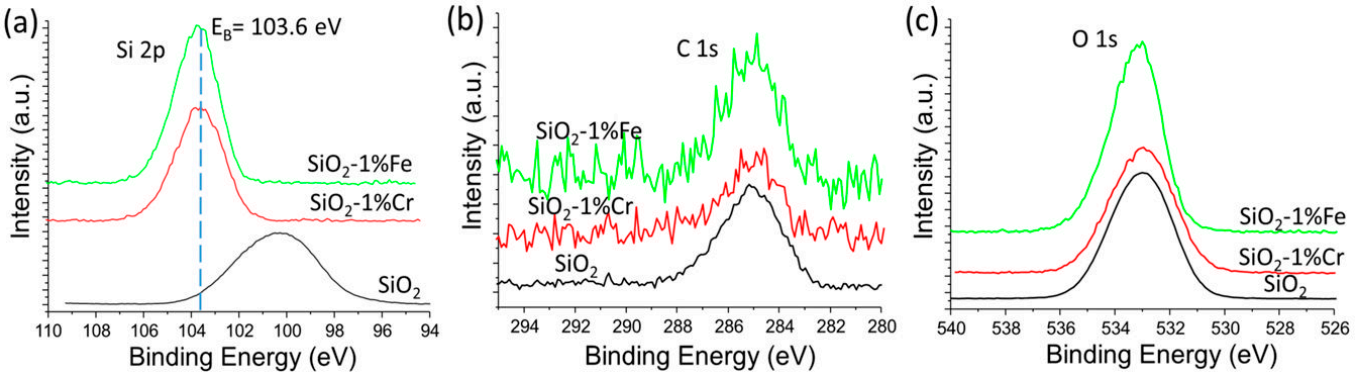


Figure 3. The Si2p (**a**), C1s (**b**) and O1s (**c**) core levels obtained for the tested samples. The blue dotted line represented the localization of the main Si2p peak in relation to the binding energy of silicon for SiO_2 compound; E = 103.6 eV.

The deconvoluted core lines of Fe2p and Cr2p, presented in Figure 4a,b, reveal a complex structure of the measured electronic states of iron and chromium. Both spectra consist of two peaks localized at 712.5 eV, 726.8 eV for iron and 578.4 eV, 586.4 eV for chromium, with binding energies related to spin-orbit coupling for the 2p state of 3d elements. The deconvolution of the Fe2p photoemission line presented in Figure 4a reveals the presence of mixed Fe^{2+} and Fe^{3+} oxidation states with contributions of about 20% and 80%, respectively. The lower binding energy position of the $Fe2p_{3/2}$ component and the presence of the feature at 718 eV in Figure 4a suggest the presence mainly of Fe^{3+} ions in the sample. The Cr2p line shape, on the other hand, is more complex and contains two doublets of components. The first one, with a lower binding energy, may indicate the presence of chromium in the metallic state, while the second doublet suggests the presence of Cr^{3+} in the test sample.

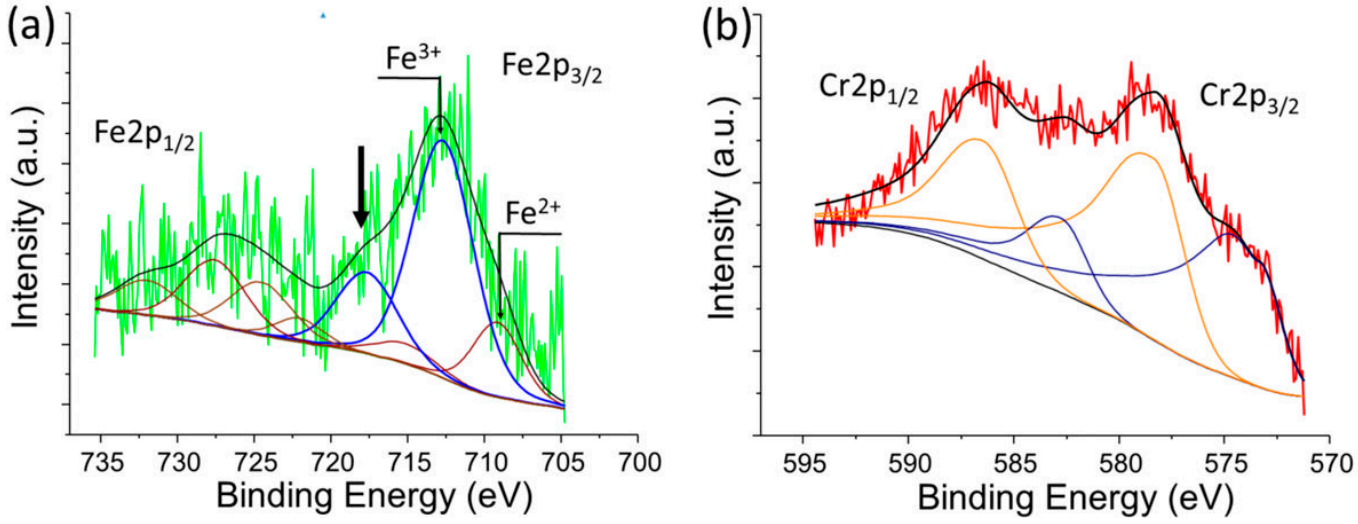


Figure 4. Deconvoluted spectra of the Fe2p (**a**) and Cr2p (**b**) core levels. The cherry lines represented Fe^{2+} valency, the blue lines are related to the electronic state with Fe^{3+} valency and the black line shown the result of fitting procedure. The black arrow indicates a characteristic feature in the shape of the spectrum at 718 eV energy, which suggests the presence of Fe^{3+} iron in the test sample. The blue lines represented metallic state of chromium, the orange lines are related to the electronic state with Cr^{3+} valency and the black line shown the result of fitting procedure. The background Shirley was fitted to both results and was subtracted for the Fe2p spectrum.

Figure 5 presents the TEM results of the studied Cr and Fe deposited on the SiO_2 nanospheres. The top row (panels a–c) shows SiO_2 material containing approximately 1 wt% chromium. The bright field (BF-TEM) image (Figure 5a) shows an almost perfectly spherical silica microsphere. The average microsphere diameter is 392(29) nm estimated based on the manual size analysis of 80 particles. The sphere's interior is uniformly darkened, corresponding to an amorphous SiO_2 with thickness that gradually increases toward the center. One recognizes delicate, undulating ribbons only a few nanometers thick—thin chromium flakes on its surface and surrounding area. The absence of any sharply defined nanocrystallites demonstrates the high degree of dispersion of the metallic phase. This is confirmed by the SAED pattern (Figure 5b). Only two broad, fuzzy diffraction rings accompany the central transmission spot. The lack of sharp reflections indicates that the SiO_2 core and the chromium-containing layer remain amorphous. The strongest diffraction halo corresponds to the average near-neighbor distance in vitreous SiO_2; the weaker outer ring can be attributed to short-range correlations in the Cr-O lattice. The chemical composition of the area analyzed was performed using EDX spectroscopy (Figure 5c).

The dominant signal is Si-Kα (1.74 keV) and O-Kα (0.52 keV), confirming a silica matrix. Distinct Cr-Kα/β peaks (5.41 keV and 5.95 keV) attest to the presence of chromium, while trace C and Cu signals come from the TEM grid. The Si:Cr intensity ratio reaches tens to one, corresponding to a nominal loading of 1 wt%.

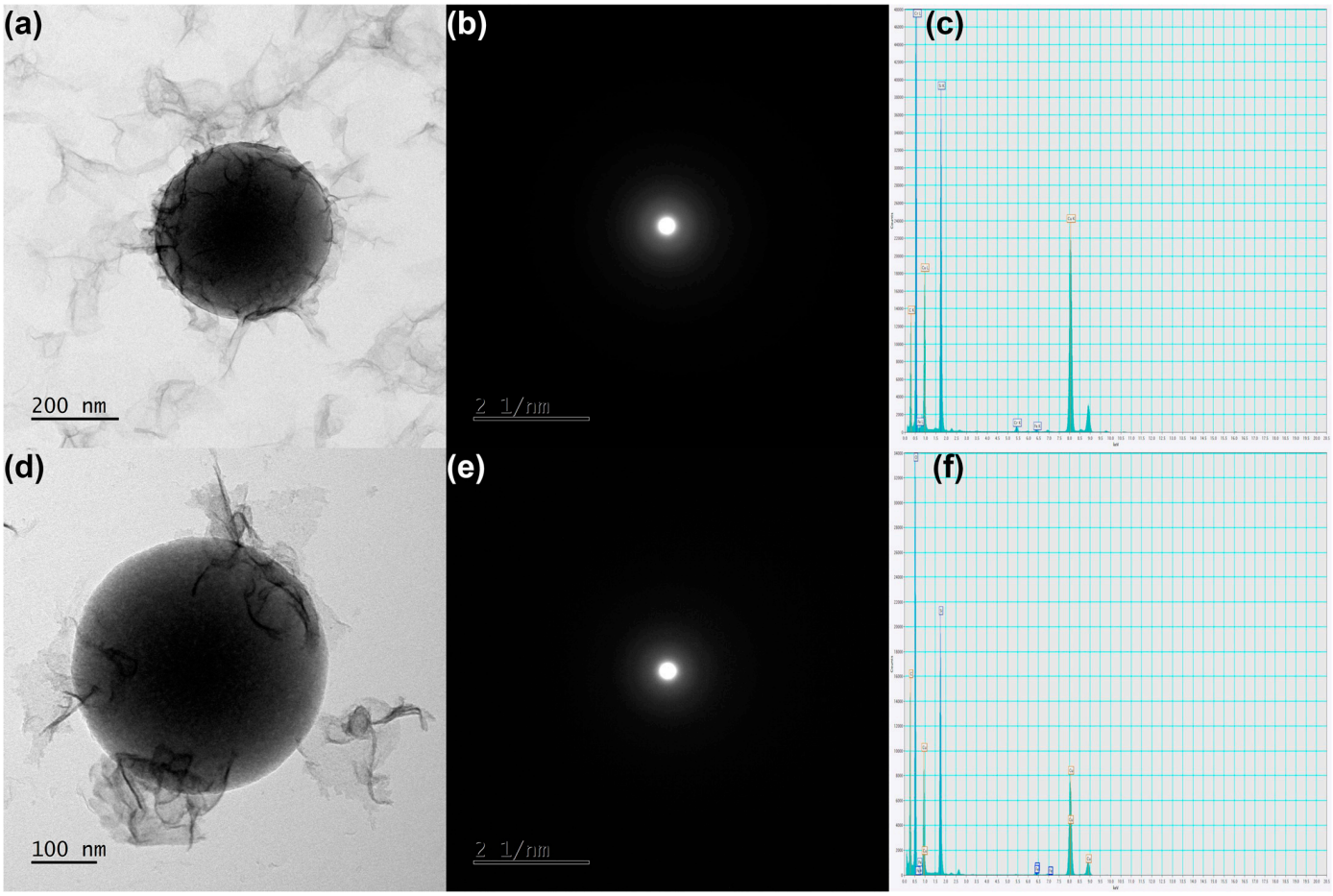


Figure 5. Upper row: Cr/SiO_2 sample: (**a**) BF-TEM image of a spherical particle (200 nm scale), (**b**) corresponding SAED pattern and (**c**) EDX spectrum. Bottom row: Fe/SiO_2 sample: (**d**) BF-TEM image of a spherical particle (100 nm scale), (**e**) corresponding SAED pattern and (**f**) EDX spectrum.

The bottom row relates to an analogous material with approximately 1 wt% iron. In the TEM image (Figure 5d), the SiO_2 microsphere is equally monodisperse. More undulating, locally thicker lamellae are observed on their surface, interpreted as amorphous iron deposited as nanoscopic flakes. The entire core retains a continuous contrast and the lack of bright edges indicates no crystalline agglomerates of hematite or magnetite have formed in the studied fragment. The SAED (Figure 5e) shows an identical pattern to chromium: a strong central spot plus a fuzzy halo, demonstrating the completely amorphous nature of both the silica and the Fe flakes. The EDX spectrum (Figure 5f) contains the dominant Si-Kα and O-Kα signals and distinct Fe-Kα (6.40 keV) and Fe-Kβ (7.06 keV) peaks. The intensity of the iron lines here is slightly higher than the chromium lines in the sample above, suggesting a thicker local Fe layer, with visible C and Cu signals from the substrate. As shown in Tables S2 and S3, Supplementary Materials, we collected the TEM-EDS quantitative analysis of Cr and Fe NPs embedded in silica gel (sol-gel), which confirmed the qualitative and quantitative EDXRF analysis (Table 3). The results indicate that the two techniques are both consistent and complementary in determining the sample composition with respect to the analyzed elements.

For comparison purposes, the 1.0% Cr/SiO_2 and 1.0% Fe/SiO_2 catalysts were tested in a model acetalization reaction of three structurally similar polyols in directly reacting with acetone. Results are summarized in Table 4. The conversion rate, selectivity and yield of the synthesized cyclic ketals depend on the polyol structure sequencing in the following order: glycerol > propylene glycol > ethylene glycol. In each analyzed case, the highest activity was observed for Cr NPs. Comparing the TON parameter values for Cr NPs vs. Fe NPs, it was observed that the differences were the largest in the glycerol–acetone system 859 vs. 427, respectively, and the smallest in the ethylene glycol–acetone system 563 vs. 436, respectively (Table 4, entries 3, 4 vs. 11, 12). Moreover, in the glycerol–acetone system, a higher selectivity of the synthesis of the main product was observed for 1.0% Cr/SiO_2 than for 1.0% Fe/SiO_2, 92.5% vs. 60.2%, respectively (Table 4, entry 3 vs. 4). The systems with propylene and ethylene glycol were characterized by comparable selectivity of the synthesis of the main products, 96.7% vs. 100% and 94.7% vs. 95.6%, respectively (Table 4, entries 7, 8 vs. 11, 12). For comparative purposes, we also tested the catalyst reusability. The results are summarized in Table S4, Supplementary Materials. Three consecutive cycles were tested for the same catalyst batch, resulting in DMD yield synthesis decreases between cycle I vs. cycle III an 8.4% for 1.0% Cr/SiO_2 and 32.6% for 1.0% Fe/SiO_2, respectively. The decrease in catalyst activity was primarily due to nanoparticle leaching during the reaction, which is a natural consequence of liquid-phase reactions. In summary, 1.0% Cr/SiO_2 proved to be the most effective catalyst for larger-scale applications, while 1.0% Fe/SiO_2 served as a cost-efficient, single-use alternative. Cr/SiO_2 catalysts are widely used in industrial processes [63], and our first reported application of Cr NPs in polyol acetalization demonstrates the potential for efficient scaling of 1,3-dioxolane synthesis.

Table 4. Catalytic performance of series of Cr or Fe NPs deposited at sol-gel silica in polyols acetalization with acetone [a].

Entry	Catalyst [a]	Reagents	α [b] [%]	TON [c]	Selectivity [%] [d]		Yield [%] [d]	
					CK	OS	CK	OS
1	Blank test	glycerol—acetone	0	0	0 [I]	0	0 [I]	0
2	SiO_2		5.1	0	0 [I]	100	0 [I]	5.1
3	1.0% Fe/SiO_2		30.6	427	60.2 [I]	39.8	18.4 [I]	12.2
4	1.0% Cr/SiO_2		66.1	859	92.5 [I]	7.5	61.1 [I]	5.0
5	Blank test	propylene glycol—acetone	1.8	0	0 [II]	100	0 [II]	1.8
6	SiO_2		2.0	0	0 [II]	100	0 [II]	2.0
7	1.0% Fe/SiO_2		28.7	401	96.7 [II]	3.3	28 [II]	0.9
8	1.0% Cr/SiO_2		52.3	680	100 [II]	0	52.3 [II]	0
9	Blank test	ethylene glycol—acetone	1.3	0	0 [III]	100	0 [III]	1.3
10	SiO_2		1.3	0	0 [III]	100	0 [III]	1.3
11	1.0% Fe/SiO_2		31.2	436	94.7 [III]	5.3	30 [III]	1.7
12	1.0% Cr/SiO_2		43.3	563	95.6 [III]	4.4	41.4 [III]	1.9

[a] Reaction conditions: 1.21 mol/L propylene glycol or 1.24 mol/L ethylene glycol or 1.23 mol/L glycerol concentration in the reaction mixture with acetone, 20 mg of catalyst, ultrasound homogenization 1 min, 55 °C, 1 h, 200 rmp. [b] α—conversion rate. [c] Turnover number (TON) based on the total metal NPs content in the material calculated based on equation [37]. [d] CK—main product cyclic ketal, ([I]—(2,2-dimethyl-1,3-dioxolan-4-yl)methanol—solketal; [II]—2,2,4-trimethyl-1,3-dioxolane; [III]—2,2-dimethyl-1,3-dioxolane), OS—other intermediate products.

The catalysts with Fe or Cr NPs were tested for the possibility of DMD (2,2-dimethyl-1,3-dioxolane) synthesis in the direct reaction of acetone with gelatin dehydrated ethylene glycol solutions (standard solutions of 5, 10, 20, 40, 60, 80 and 99 wt%). Figure 6 presents the results of DMD synthesis yield for 1.0% Cr/SiO_2 or 1.0% Fe/SiO_2 in the absence and presence of the acidic ion exchange resin Amberlyst 15H. Catalysts without the addition of acidic ion exchange resin in the range of ethylene glycol concentrations of 5–60 wt% allow DMD synthesis with a 2.2–14.9% yield. Exceeding the concentration of ethylene glycol in the sample above 60% causes a rapid increase in DMD synthesis yield up to 40%. Fe NPs (blue continuous line) demonstrated higher activity in such reaction conditions than Cr NPs (red continuous line). The addition of Amberlyst 15H resin increased the yield of DMD synthesis. For ethylene glycol solutions with a concentration of 5–50%, the DMD synthesis yield increased by 12.2–29.5%, and after exceeding the concentration of ethylene glycol in the sample up to 60 wt%, DMD synthesis was possible with a yield of up to 50.5%. Contrary to the previous case, a greater increase in the activity of Cr NPs (red dotted line) was observed than that of Fe NPs (blue dotted line). In summary, regardless of the catalyst used, the overall dependence of DMD synthesis yield strongly depends on the amount of water in the sample. A large amount of water inhibits the reaction and affects the shift of the reaction equilibrium to the left.

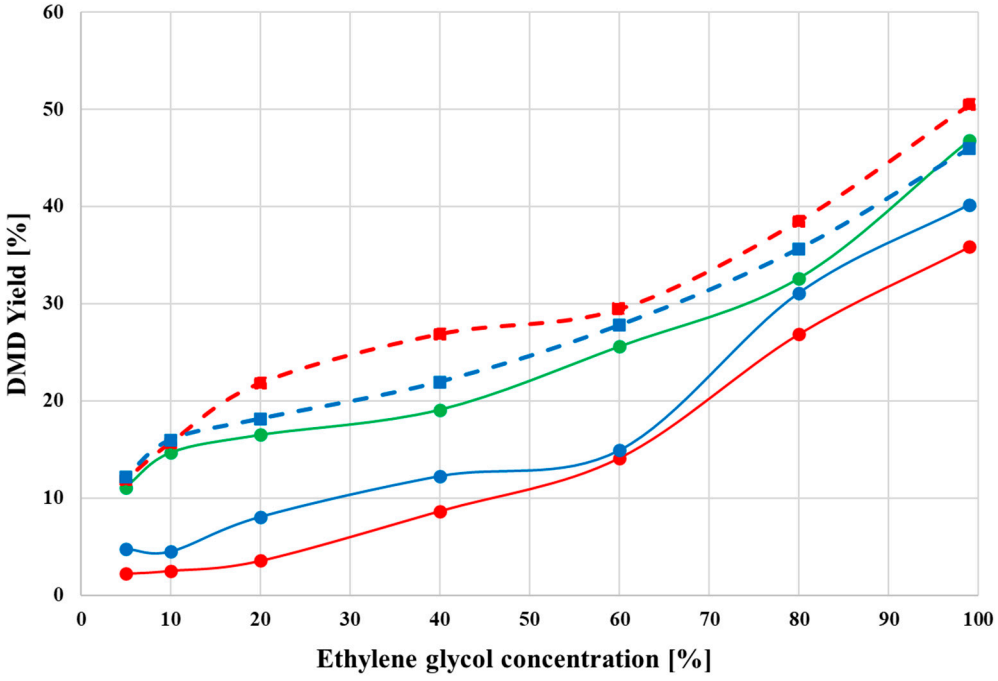


Figure 6. The influence of ethylene glycol concentration of DMD—2,2-dimethyl-1,3-dioxolane synthesis yield for selected experimental variants: 1.0% Cr/SiO_2 and Amberlyst 15H dehydrated with gelatine (■) 1.0% Fe/SiO_2 and Amberlyst 15H dehydrated with gelatine (■), Amberlyst 15H (●), 1.0% Cr/SiO_2 (●) and 1.0% Fe/SiO_2 (●).

According to Scheme 1, after pressure hydrolysis and rPET flake depolymerization, the liquid fraction was dehydrated with gelatin, separating the ethylene glycol solution for further DMD synthesis. Table 1 presents the test results for 1.0% Fe/SiO_2 and 1.0% Cr/SiO_2 catalysts without and in the presence of Amberlyst 15H for different reaction conditions. The 1.0% Cr/SiO_2 catalyst was tested for three solutions at successively increasing temperatures of 30, 40 and 50 °C, respectively, with a gradual extension of the reaction time from 30 to 90 min (Table 5, entries 1, 3, 5). For the gelatin-dehydrated solution after rPET hydrolysis (PET:H_2O = 40:40), the highest DMD synthesis yield of 16.0% was observed,

while the synthesis yield without DMD dehydration was 13.7% (Table 5, entry 3). The same solution in the presence of 1.0% Fe/SiO_2 catalyst allowed for DMD synthesis yield for the gelatin-dehydrated vs. non-dehydrated solution of 13.1% vs. 9.5%, respectively (Table 5, entry 4). Under comparable reaction conditions (temperature and catalyst amount) a high proportion of water in the sample after hydrolysis (PET:H_2O = 10:40) causes a significant reduction in the DMD synthesis yield. For example, for 1.0% Cr/SiO_2 the DMD synthesis yield for the gelatin-dehydrated vs. non-dehydrated sample was 9.6% vs. 8.2%, respectively (Table 5, entry 5) and for 1.0% Fe/SiO_2 6.8% vs. 6.1%, respectively (Table 5, entry 6). Comparing the DMD synthesis capabilities of both catalysts at low water content in the sample after hydrolysis (PET:H_2O = 40:30), almost doubling the process temperature results in more than doubling the efficiency. The 1.0% Fe/SiO_2 catalyst at 60 °C allowed to obtain a yield for the dehydrated vs. non-dehydrated sample of 13.8% vs. 9.6% (Table 5, entry 2), respectively, while the 1.0% Cr/SiO_2 catalyst at 30 °C allowed to synthesize DMD with the efficiency of 6.2% vs. 6.1%, respectively (Table 5, entry 1). The key factors are the process temperature, the water content of rPET after hydrolysis and the degree of sample gelatin-dehydration. The Cr NPs are much more active than the Fe NPs, e.g., Cr activation is visible at 40 °C (Table 5, entry 1 vs. 3), while Fe NPs require 55 °C (Table 5, entry 2 vs. 4).

Table 5. Basic parameters of the processing of the liquid residue after pressure hydrolysis of rPET with the determination of the yield of the 2,2-dimethyl-1,3-dioxolane (DMD) synthesis process.

Entry	Hydrolysis		Dehydration			Reactions Conditions	DMD Yield [%]
	rPET [g]	Water [mL]	Sol. vol. [mL]	Gelatine [g]	Swelling Time [h]		
1	40	30	15	0.85	0.5	10 mg Amberlyst 15H, 20 mg 1% Cr/SiO_2, sol.: AcMe ratio = 1.0 mL:14.0 mL, 35 °C, 30 min, 150 rpm	6.2 [I] vs. 6.1 [II]
2	40	30	15	0.85	0.5	10 mg Amberlyst 15H, 30 mg 1% Fe/SiO_2, sol.: AcMe ratio = 0.6 mL:6.0 mL, 60 °C, 45 min, 400 rpm	13.8 [I] vs. 9.6 [II]
3	40	40	20	0.60	1.5	10 mg Amberlyst 15H, 50 mg 1% Cr/SiO_2, sol.: AcMe ratio = 0.58 mL:5.76 mL, 40 °C, 90 min, 300 rpm	16.0 [I] vs. 13.7 [II]
4	40	40	20	0.60	1.5	10 mg Amberlyst 15H, 40 mg 1% Fe/SiO_2, sol.: AcMe ratio = 1.0 mL:9.0 mL, 55 °C, 60 min, 200 rpm	13.1 [I] vs. 9.5 [II]
5	10	40	21	0.84	2.0	10 mg Amberlyst 15H, 10 mg 1% Cr/SiO_2, sol.: AcMe ratio = 0.58 mL:4.06 mL, 50 °C, 180 min, 250 rpm	9.6 [I] vs. 8.2 [II]
6	10	40	21	0.84	2.0	10 mg Amberlyst 15H, 10 mg 1% Fe/SiO_2, sol.: AcMe ratio = 1.0 mL:5.0 mL, 57 °C, 210 min, 300 rpm	6.8 [I] vs. 6.1 [II]

[I] post-reaction solution dehydrated with gelatine; [II] comparative test the post-reaction solution was used immediately after the reaction without dehydration with gelatin. Acronyms: sol.—solution; vol.—volume; AcMe—acetone.

We investigated the solubility studies of polymers, foam and glue in 1,3-dioxolanes at room temperature. Table 6 specifies the results. No changes were observed after

48 h for rPET (recycled poly(ethylene terephthalate) in flakes and crushed form, PEN (poly(ethylene naphthalene-2,6-dicarboxylate)), PP (poly(propylene)) and HDPE (high density poly(ethylene)) in crushed form (no solubility). Dissolution after one hour was recorded for PMMA (poly(methylene methacrylate) and two-component epoxy glue for 2,2-dimethyl-1,3-dioxolane. The 2,2,4-trimethyl-1,3-dioxolane dissolved two-component epoxy glue in one hour and PMMA in five hours. We observed swelling (increase in volume) of PMMA and TMD and (2,2-dimethyl-1,3-dioxolane-4-yl)methanol and polyurethane foam for all 1,3-dioxolanes. A change in the color of the polyurethane foam appeared after 24 h in the case of DDM. Adding an additional 1 cm^3 of DDM to the polyurethane foam did not affect the system—the solution remained clear. No dissolution of the polyurethane foam was recorded after 48 h (no changes even after 84 h). The best solvent among the presented 1,3-dioxolane derivatives is DMD in the case of PMMA polymer and two-component epoxy glue.

Table 6. Basic data for 1,3-dioxolane derivatives applications as organic solvents for selected groups of polymers. Acronyms: (DMD) 2,2-dimethyl-1,3-dioxolane; (TMD) 2,2,4-trimethyl-1,3-dioxolane; (DDM) (2,2-dimethyl-1,3-dioxolane-4-yl)methanol—solketal.

Polymer (Form)/Foam/Glue	TMD	DDM	DMD
rPET flakes [1]	-- 48h	-- 48h	-- 48h
rPET in crushed form Fraction $\leq$ 1 mm	-- 48h light blue color of the solution 2min	-- 48h blue thick solution 2min	-- 48h light blue color of the solution 2min
PMMA in powdered form [2]	Swell 2h cloudy solution 1h +- 3h ++ 5h	Swell 1h cloudy solution 45min +- 5h ++ 24h	++ 1h
PEN in crushed form Fraction $\leq$ 1 mm	-- 48h light blue color of the solution 2min	-- 48h light blue color of the solution 2min	-- 48h light blue color of the solution 2min
Polyurethane foam [3]	swell 2min after 2 min no visible solution	swell 5min after 5 min partial disappearance of solution after 30 min no visible solution	swell 2min after 2 min no visible solution
Two-component epoxy glue [3]	cloudy solution 0min +- 15min ++ 1h milky color	cloudy solution 5min +- 30min milky color	cloudy solution 2min +- 15min ++ 1h milky color
HDPE in crushed form Fraction $\leq$ 1 mm	-- 48h	-- 48h	-- 48h
PP in crushed form Fraction $\leq$ 1 mm	-- 48h	-- 48h	-- 48h

[1]—form supplied by the recycling company, [2]—form supplied by the manufacturer (Mw $\approx$ 15,000, Sigma-Aldrich 200336), [3]—solubility test after 24 h, after full curing, ++—dissolves in room temperature, +—-partially dissolves in room temperature, -—-does not dissolve in room temperature, the time is given in the superscript.

The solid residue after hydrolysis of rPET flakes, mainly crude terephthalic acid, is utilized as shown in Scheme 1. Purified terephthalic acid (purity 98.5% DSC technique, Figure S4, Supplementary Materials), following the methodology described in Section 2.5, can be used as a secondary raw material for PET synthesis (bottles or consumables for thermoplastic molding). The possibility of using crude terephthalic acid as an additive to B-20 concrete in the amount of 3.5 wt% was also checked (detailed described in Sections 2.7 and 2.8). Table 7 presents the results of the sample compressive strength (R_c) and the percentage reduction of the sample mass (Mass red.) concerning the reference sample ($1^{ref.}$). For comparative purposes, the influence of crushed PET on the properties of B-20 concrete, widely described in the literature, was also checked [59,64–66]. Comparing the reference sample, the addition of 3.5 wt% of ground rPET fractions 0.25 mm vs. < 1 mm causes the increase of the compressive strength of concrete B-20 by 2.94 MPa vs. 3.79 MPa vs. 4.51 MPa, respectively (Table 7, entries $1^{ref.}$ vs. 2 vs. 3). The effect of the admixture of concrete with rPET fraction < 1 mm vs. 0.25 mm resulted in a decrease in the mass of the samples by 4.2% vs. 4.7%, respectively. The addition of unpurified terephthalic acid directly to concrete resulted in the release of a large amount of heat (acid–base reaction), increased plasticity and faster hardening of concrete, and consequently the compressive strength R_c was lower in comparison to the reference sample (1.35 MPa vs. 2.94 MPa); however, the sample with the addition of terephthalic acid was 11.3% lighter (Table 7, entry 4 vs. $1^{ref.}$). The change of the sample preparation strategy, consisting of prior neutralization of the sample with 25% NH_3 (Table 7, entry 5) and additional use of gelatin as an emulsifier (Table 7, entry 6), decreased the thermal effect. As a result, the sample mass was reduced by 14.1% and 23.4%, respectively. However, with a further deterioration of the compressive strength of 0.85 MPa vs. 0.42 MPa, respectively (Table 7, entry 5 vs. 6). We also prepared a sample in which half of the terephthalic acid content was replaced by < 1 mm fraction of ground rPET. A minor mass reduction was observed for the sample containing a sole terephthalic acid addition, 13.5% vs. 11.3%, respectively. However, this came with lower compressive strength values of 0.80 MPa vs. 1.35 MPa, respectively (Table 7, entry 7 vs. 4). In summary, the main advantage of the samples doped with terephthalic acid is the reduced mass in relation to the reference sample and the samples with the addition of ground rPET (Table 7, entries $1^{ref.}$–3 vs. 4–6). Concrete can be used to produce garden ornaments, for which compressive strength is not a decisive parameter, unlike in construction applications. The main advantage of the solution is also the reduction of CO_2 resulting from the replacement of 3.5 wt% of B-20 concrete with the addition of unpurified terephthalic acid from rPET hydrolysis, without the need for its further purification.

Table 7. The parameters of modified B-20 concrete with 3.5 wt% additives of recycled rPET and terephthalic acid.

Entry	Avg. Mass [g]/Std.	Mass Red. [%]	Rc [MPa]/Std.
$1^{ref.}$	367.708 ± 2.867	0	2.94 ± 0.50
2	350.442 ± 3.115	4.7	3.79 ± 0.69
3	352.284 ± 2.296	4.2	4.51 ± 0.81
4	326.078 ± 9.185	11.3	1.35 ± 0.53
5	315.774 ± 6.044	14.1	0.85 ± 0.24
6	281.796 ± 1.254	23.4	0.42 ± 0.06
7	318.034 ± 10.239	13.5	0.80 ± 0.06

Acronyms: $^{ref.}$—reference sample; Avg. mass—average mass of three concrete cylinders with 3.5 wt% additives from Table 2; R_c—compressive strength; Std.—standard deviation; Mass red.—percentage of reduction in the mass of a concrete cylinder in relation to the reference sample.

4. Executive Summary and Conclusions

Catalytic methods for processing waste PET [7,12,27,67–70] are currently regarded as promising strategies for the reduction of polymer waste, however, they do not primarily address the minimization of secondary post-processing waste generation. This article presents a comprehensive approach to rPET management with zero waste generation (Scheme 1). The neutral-pH pressure hydrolysis of rPET generates two fractions, solid and liquid. We can rationally manage these fractions to produce products with higher added value.

The solid fraction, mainly terephthalic acid, has been purified to 98.5%, allowing its reuse for PET synthesis or thermoplastic molding. On the other hand, unpurified terephthalic acid (up to 3.5 wt%) used as an additive can reduce concrete mass in the range 11.3–23.4%. The main limitation of organic additives to concrete is the decrease in the material's compressive strength. Modified concrete can be applied to produce garden ornaments, for which compressive strength is not a decisive parameter, as in construction applications. Lower mass may be a valuable feature for the end user, due to easier transport of decorations and garden arrangement and the lower final product price. From an environmental perspective, using terephthalic acid through concrete mass directly saves energy and resources needed for concrete production and, in the end, reduces CO_2 emissions.

After neutral-pH pressure hydrolysis of rPET, the liquid fraction contains ethylene glycol, which, after dehydration, is a valuable material for synthesizing 2,2-dimethyl-1,3-dioxolane (DMD). The most popular methods of ethylene glycol separation from aqueous solutions are based on membranes, e.g., reverse osmosis or pervaporation techniques. In this research, we proved that it is possible to dehydrate ethylene glycol in the presence of gelatin. Due to insoluble impurities in the mixture after hydrolysis, they can be precipitated in the presence of gelatin by adding acetone, which is also a substrate for the DMD synthesis. The 1.0% Fe/SiO_2 and 1.0% Cr/SiO_2 nanocatalysts for the direct DMD synthesis process were used for the first time. The most active system was 1.0% Cr/SiO_2, a readily available catalyst widely used in industry, mainly in ethylene polymerization and oxidation processes (benzophenone, diphenylmethane and ethanol). The application of heterogeneous catalysts significantly improves the possibilities of the liquid fraction processing process, due to the easy separation of the catalyst from the post-reaction mixture. The catalysts also enable the synthesis of other cyclic ketals in the direct reaction of glycerol or propylene glycol with acetone. The developed method also allows for solving the problem of acetone oversupply, which is a by-product of the phenol synthesis process using the cumene method. After separation, the synthesis products (DDM, DMD and TMD) were tested as polar aprotic solvents of three polymer groups: polyesters, polyurethanes and epoxy resins. The best solvent was DMD, which proved excellent for two-component epoxy resin glue. Moreover, DMD, in particular, is a valuable fuel additive and adjuvant described in the literature, broadening the application areas of this compound and making the developed rPET management process more economically justified. This approach to PET recycling management aligns with the circular economy promoted by the United Nations Agenda 2030 and fits into the CO_2 anthropogenic footprint reduction goals.

5. Patents

Maciej Kapkowski, Mateusz Korzec, Sonia Kotowicz, Karina Kocot has Polish patent application no. P.446786 pending to University of Silesia.

Mateusz Korzec, Sonia Kotowicz, Maciej Kapkowski has Polish patent application no. P.446378 pending to University of Silesia.

Supplementary Materials: The following supporting information can be downloaded at: https://www.mdpi.com/article/10.3390/en18164375/s1, Figure S1: The effect of precipitation of gelatin with acetone from standard aqueous solutions of ethylene glycol. Figure S2: Reaction scheme with summary of the conditions of the pressure hydrolysis process of rPET and ^{1}H NMR spectra (Bruker Avance 500 MHz, DMSO) for samples 1–3 from Table 1, (a) solid residue, (b) liquid residue (filtrate). Figure S3: Terephthalic acid purification stages. Comparisons of superimposed NMR spectra of terephthalic acid from the pressure hydrolysis process (PET:H_2O = 30:40) before and after purification (a) ^{1}H NMR and (b) ^{13}C NMR (Bruker Avance 500 MHz, DMSO). Scheme S1: Mass distribution diagram in the rPET hydrolysis process. Figure S4: (a) The DSC thermogram of terephthalic acid under nitrogen with a heating and cooling rate of 10 °C/min in the aluminum pan in the range of 10 °C–360 °C, exo down (TA DSC 25 Discovery) and (b) thin layer chromatography (TLC) of purified terephthalic performed in chloroform ($CHCl_3$), ethanol (EtOH) and methanol (MeOH) and solid support: *silica gel 60* F_{254}. The photos were taken under UV lamp at excitations of 254 and 365 nm. Figure S5: Deconvoluted spectra of the Si2p for measured samples. The additional components are related to the spin orbit $2p_{3/2}$ and $2p_{1/2}$ coupling. Table S1: Horizontal comparison of the technical advantages of variety PET disposal methods. Table S2: TEM-EDS quantitative analysis of Cr NPs deposited at sol-gel silica. Table S3: TEM-EDS quantitative analysis of Fe NPs deposited at sol-gel silica. Table S4: Catalysts reusability and possibilities of regeneration after three cycles of the same batch of 1.0% Fe/SiO_2 or 1.0% Cr/SiO_2.

Author Contributions: Conceptualization, M.K. (Maciej Kapkowski); methodology, M.K. (Maciej Kapkowski), M.Z., K.A., J.K., S.K., K.K. and M.K. (Mateusz Korzec); software, U.S.; validation, S.K., M.K. (Mateusz Korzec) and K.K.; formal analysis, M.K. (Maciej Kapkowski), T.S., U.S. and J.P.; investigation, M.K. (Maciej Kapkowski), M.Z., K.A., J.K., S.K., K.K. and M.K. (Mateusz Korzec); resources, M.K. (Maciej Kapkowski); data curation, M.K. (Maciej Kapkowski), M.Z., K.A., J.K., S.K., K.K. and M.K. (Mateusz Korzec); writing—original draft preparation, M.K. (Maciej Kapkowski), M.Z., K.A., J.K., S.K., K.K., J.P. and M.K. (Mateusz Korzec); writing—review and editing, M.K. (Maciej Kapkowski); visualization, U.S. and T.S.; supervision, M.K. (Maciej Kapkowski) and J.P.; project administration, M.K. (Maciej Kapkowski); funding acquisition, M.K. (Maciej Kapkowski). All authors have read and agreed to the published version of the manuscript.

Funding: This research was founded by The National Centre for Research and Development grant LIDER XI No. LIDER/39/0137/L-11/19/NCBR/2020.

Data Availability Statement: The original contributions presented in this study are included in the article and Supplementary Materials. Further inquiries can be directed to the corresponding author.

Acknowledgments: J.P. thanks the University of Silesia project: Widzialność Centrów Badawczych, w Mieście Nauki.

Conflicts of Interest: The authors declare no conflicts of interest. The funders had no role in the design of the study; in the collection, analyses, or interpretation of data; in the writing of the manuscript; or in the decision to publish the results.

References

1. Report Future Market Insigns, Polyethylene Terephthalate Market Growth—Trends & Forecast 2025 to 2035. Available online: https://www.futuremarketinsights.com/reports/polyethylene-terephthalate-market (accessed on 7 July 2025).
2. Tamburini, E.; Krozer, Y.; Castaldelli, G. How Much Are We Paying for Drinking Water in (PET) Bottles? A Global Assessment of the Hidden Costs and Potential Damage to the Environment. *Environ. Chall.* **2025**, *18*, 101083. [CrossRef]
3. Sax, L. Polyethylene Terephthalate May Yield Endocrine Disruptors. *Environ. Health Perspect.* **2010**, *118*, 445–448. [CrossRef]
4. Wagner, M.; Oehlmann, J. Endocrine Disruptors in Bottled Mineral Water: Total Estrogenic Burden and Migration from Plastic Bottles. *Environ. Sci. Pollut. Res.* **2009**, *16*, 278–286. [CrossRef]
5. Cramer, A.; Benard, P.; Zarebanadkouki, M.; Kaestner, A.; Carminati, A. Microplastic Induces Soil Water Repellency and Limits Capillary Flow. *Vadose Zone J.* **2023**, *22*, e20215. [CrossRef]
6. Chu, M.; Tu, W.; Zhang, Q.; Huang, W.; Chen, J.; Ma, D. Co-Recycling of Plastics and Other Waste Materials. *Nat. Rev. Clean. Technol.* **2025**, *1*, 320–332. [CrossRef]

7. Kumar, V.; Sharma, N.; Umesh, M.; Janghu, P.; Sarojini, S.; Chakraborty, P.; Pasrija, R. Methods and Techniques to Fabricate PET Recycled Nanomaterials: A Review. *J. Mater. Cycles Waste Manag.* **2025**, *27*, 2076–2098. [CrossRef]
8. Hahladakis, J.N.; Iacovidou, E. An Overview of the Challenges and Trade-Offs in Closing the Loop of Post-Consumer Plastic Waste (PCPW): Focus on Recycling. *J. Hazard. Mater.* **2019**, *380*, 120887. [CrossRef] [PubMed]
9. Yang, W.; Liu, R.; Li, C.; Song, Y.; Hu, C. Hydrolysis of Waste Polyethylene Terephthalate Catalyzed by Easily Recyclable Terephthalic Acid. *Waste Manag.* **2021**, *135*, 267–274. [CrossRef]
10. Gallardo-Sánchez, M.A.; Chinchillas-Chinchillas, M.J.; Gaxiola, A.; Alvarado-Beltrán, C.G.; Hurtado-Macías, A.; Orozco-Carmona, V.M.; Almaral-Sánchez, J.L.; Sepúlveda-Guzmán, S.; Castro-Beltrán, A. The Use of Recycled PET for the Synthesis of New Mechanically Improved PVP Composite Nanofibers. *Polymers* **2022**, *14*, 2882. [CrossRef] [PubMed]
11. Kotowicz, S.; Korzec, M.; Kapkowski, M.; Pająk, A.K. Photophysical Investigations of the Organic Compounds Synthesised from Waste Poly(Ethylene Terephthalate). *Ecol. Chem. Eng. S* **2024**, *31*, 253–266. [CrossRef]
12. Guo, Z.; Wu, J.; Wang, J. Chemical Degradation and Recycling of Polyethylene Terephthalate (PET): A Review. *RSC Sustain.* **2025**, *3*, 2111–2133. [CrossRef]
13. Umdagas, L.; Orozco, R.; Heeley, K.; Thom, W.; Al-Duri, B. Advances in Chemical Recycling of Polyethylene Terephthalate (PET) via Hydrolysis: A Comprehensive Review. *Polym. Degrad. Stab.* **2025**, *234*, 111246. [CrossRef]
14. Al-Salem, S.M.; Antelava, A.; Constantinou, A.; Manos, G.; Dutta, A. A Review on Thermal and Catalytic Pyrolysis of Plastic Solid Waste (PSW). *J. Environ. Manag.* **2017**, *197*, 177–198. [CrossRef]
15. Shanker, R.; Khan, D.; Hossain, R.; Islam, M.T.; Locock, K.; Ghose, A.; Sahajwalla, V.; Schandl, H.; Dhodapkar, R. Plastic Waste Recycling: Existing Indian Scenario and Future Opportunities. *Int. J. Environ. Sci. Technol.* **2023**, *20*, 5895–5912. [CrossRef]
16. Kawai, F. Emerging Strategies in Polyethylene Terephthalate Hydrolase Research for Biorecycling. *ChemSusChem* **2021**, *14*, 4115–4122. [CrossRef]
17. Kotowicz, S. Charakterystyka Folii Otrzymanych z Recyklingowanego Poli(Tereftalanu Etylenu). *Chem. Rev.* **2025**, *1*, 68–72. [CrossRef]
18. Bushra, R.; Khayal, A.; Ahmad, M.; Song, J.; Jin, Y.; Xiao, H. Catalytic Conversion of Polymer Waste into High-Value Products for Advancing Circular Economy and Eco-Sustainability. *J. Anal. Appl. Pyrolysis* **2025**, *189*, 107052. [CrossRef]
19. Deng, L.; Guo, W.; Ngo, H.H.; Zhang, X.; Wei, D.; Wei, Q.; Deng, S. Novel Catalysts in Catalytic Upcycling of Common Polymer Wastes. *Chem. Eng. J.* **2023**, *471*, 144350. [CrossRef]
20. Cho, S.-H.; Park, J.; Lee, D.; Cho, H.; Lee, J.; Kwon, E.E. Recovery of Gaseous Fuels through CO_2-Mediated Pyrolysis of Thermosetting Polymer Waste. *Chemosphere* **2024**, *363*, 142892. [CrossRef] [PubMed]
21. Baskar, S.; Padmanabhan, S.; Raman, A.; Venkatesan, M.; Ganesan, S.; Kumar, K.M.; Mahalingam, S. A Circular Economy Approach to Energy Recovery from Polymer Waste with Oxygenated Additives as a Sustainable Fuel. *Results Eng.* **2025**, *25*, 104516. [CrossRef]
22. Ryou, H.; Byun, J.; Bae, J.; Kim, D.K.; Han, J. Energy-Efficient and Environmentally Friendly Upcycling of Waste Plastic into Fuels, Chemicals, and Polymer. *Chem. Eng. J.* **2025**, *511*, 162256. [CrossRef]
23. Roldan Cuenya, B.; Behafarid, F. Nanocatalysis: Size- and Shape-Dependent Chemisorption and Catalytic Reactivity. *Surf. Sci. Rep.* **2015**, *70*, 135–187. [CrossRef]
24. Scirè, S.; Liotta, L.F. Supported Gold Catalysts for the Total Oxidation of Volatile Organic Compounds. *Appl. Catal. B Environ.* **2012**, *125*, 222–246. [CrossRef]
25. Shi, J. On the Synergetic Catalytic Effect in Heterogeneous Nanocomposite Catalysts. *Chem. Rev.* **2013**, *113*, 2139–2181. [CrossRef]
26. Polanski, J.; Lach, D.; Kapkowski, M.; Bartczak, P.; Siudyga, T.; Smolinski, A. Ru and Ni—Privileged Metal Combination for Environmental Nanocatalysis. *Catalysts* **2020**, *10*, 992. [CrossRef]
27. Zhang, W.; Hao, X.; Liu, X.; Chu, M.; Li, S.; Wang, X.; Jiang, F.; Wang, L.; Zhang, Q.; Chen, J.; et al. Photocatalytic Conversion of Polyester-Derived Alcohol into Value-Added Chemicals by Engineering Atomically Dispersed Pd Catalyst. *Angew. Chem. Int. Ed.* **2025**, *64*, e202500814. [CrossRef]
28. Liu, Y.; Yan, P.; Li, X.; Li, Q.; Li, S.; Han, H.; Chu, M.; Fu, J.; Cao, M.; Xu, P.; et al. Selective Recycling of Mixed Polyesters via Heterogeneous Photothermal Catalysis. *Adv. Mater.* **2025**, *37*, 2412740. [CrossRef] [PubMed]
29. Kapkowski, M.; Lach, D.; Siudyga, T.; Kocot, K.; Kotowicz, S.; Korzec, M.; Bartczak, P.; Balin, K.; Zubko, M.; Dercz, G.; et al. Nano-Ru Deposited on Titanium Dioxide as Effective Photocatalyst for Synthesis of Cyclic Ketals for Application as Fuel Biocomponents. *Appl. Catal. A: Gen.* **2025**, *691*, 120066. [CrossRef]
30. Deutsch, J.; Martin, A.; Lieske, H. Investigations on Heterogeneously Catalysed Condensations of Glycerol to Cyclic Acetals. *J. Catal.* **2007**, *245*, 428–435. [CrossRef]
31. He, D.Y.; Li, Z.J.; Li, Z.J.; Liu, Y.Q.; Qiu, D.X.; Cai, M.S. Studies on Carbohydrates X. A New Method for the Preparation of Isopropylidene Saccharides. *Synth. Commun.* **1992**, *22*, 2653–2658. [CrossRef]
32. Lin, C.-H.; Lin, S.D.; Lin, T.-P.; Huang, Y.-J. The Influence of Steric and Electronic Effects on the Preparation of Cyclic Acetals Catalyzed by Sulfated Metal Oxides. *Appl. Catal. A: Gen.* **2003**, *240*, 253–262. [CrossRef]

33. He, J.; Qiang, Q.; Bai, L.; Su, W.; Yu, H.; Liu, S.; Li, C. Acetalization Strategy in Biomass Valorization: A Review. *Ind. Chem. Mater.* **2024**, *2*, 30–56. [CrossRef]
34. Kapkowski, M.; Ambrożkiewicz, W.; Siudyga, T.; Sitko, R.; Szade, J.; Klimontko, J.; Balin, K.; Lelątko, J.; Polanski, J. Nano Silica and Molybdenum Supported Re, Rh, Ru or Ir Nanoparticles for Selective Solvent-Free Glycerol Conversion to Cyclic Acetals with Propanone and Butanone under Mild Conditions. *Appl. Catal. B Environ.* **2017**, *202*, 335–345. [CrossRef]
35. Kapkowski, M.; Popiel, J.; Siudyga, T.; Dzida, M.; Zorębski, E.; Musiał, M.; Sitko, R.; Szade, J.; Balin, K.; Klimontko, J.; et al. Mono- and Bimetallic Nano-Re Systems Doped Os, Mo, Ru, Ir as Nanocatalytic Platforms for the Acetalization of Polyalcohols into Cyclic Acetals and Their Applications as Fuel Additives. *Appl. Catal. B Environ.* **2018**, *239*, 154–167. [CrossRef]
36. Mallesham, B.; Sudarsanam, P.; Reddy, B.M. Eco-Friendly Synthesis of Bio-Additive Fuels from Renewable Glycerol Using Nanocrystalline SnO2-Based Solid Acids. *Catal. Sci. Technol.* **2014**, *4*, 803. [CrossRef]
37. Kapkowski, M.; Siudyga, T.; Kocot, K.; Balin, K.; Fijałkowski, M.; Zubko, M.; Prusik, K.; Chojnowska, A.; Dercz, G.; Kujawski, W.; et al. Exploring Induction Heating Catalysis with Nano-Indium on Silica: From Room-Temperature to Thermal Synthesis of 1,3-Dioxolane as a New Sustainable Fertilizer Enhancer. *Chem. Eng. Res. Des.* **2025**, *218*, 867–885. [CrossRef]
38. Tempio, E.; Ravez, A.; Lach, D.; Kapkowski, M.; Plevova, K.; Gilles, L.; Polanski, J.; Antoniotti, S. Iron(III) Chloride-Catalyzed Acetalisation of α,β-Unsaturated Carbonyl Compounds towards Odorant Ketals. *Tetrahedron* **2023**, *149*, 133734. [CrossRef]
39. Krompiec, S.; Penkala, M.; Szczubiałka, K.; Kowalska, E. Transition Metal Compounds and Complexes as Catalysts in Synthesis of Acetals and Orthoesters: Theoretical, Mechanistic and Practical Aspects. *Coord. Chem. Rev.* **2012**, *256*, 2057–2095. [CrossRef]
40. Smirnov, A.A.; Selishcheva, S.A.; Yakovlev, V.A. Acetalization Catalysts for Synthesis of Valuable Oxygenated Fuel Additives from Glycerol. *Catalysts* **2018**, *8*, 595. [CrossRef]
41. Climent, M.J.; Corma, A.; Iborra, S. Conversion of Biomass Platform Molecules into Fuel Additives and Liquid Hydrocarbon Fuels. *Green Chem.* **2014**, *16*, 516. [CrossRef]
42. Walsh, R.H. Dioxolanes and Thio Analogs, Derivatives Thereof and Lubricants and Fuels Containing Same 1988. Available online: https://patents.google.com/patent/US4906253A/en?oq=US4906253A (accessed on 7 July 2025).
43. Mcdougall, P.J. Lubricating Composition Containing 1,3-Dioxolane-4-Methanol Compounds as Antiwear Additives. U.S. Patent 8,349,777, 8 January 2013.
44. Szwajczak, E.; Sierka, E.; Ludynia, M. Potential Role of Low-Molecular-Weight Dioxolanes as Adjuvants for Glyphosate-Based Herbicides Using Photosystem II as an Early Post-Treatment Determinant. *Cells* **2023**, *12*, 777. [CrossRef]
45. Kapkowski, M.; Ludynia, M.; Rudnicka, M.; Dzida, M.; Zorębski, E.; Musiał, M.; Doležal, M.; Polanski, J. Enhancing the CO_2 Capturing Ability in Leaf via Xenobiotic Auxin Uptake. *Sci. Total Environ.* **2020**, *745*, 141032. [CrossRef]
46. Moscoso, R.; Carbajo, J.; Squella, J.A. 1,3-Dioxolane: A Green Solvent for the Preparation of Carbon Nanotube-Modified Electrodes. *Electrochem. Commun.* **2014**, *48*, 69–72. [CrossRef]
47. Albanelli, N.; Capodarca, F.; Zanoni, M.; Lacarbonara, G.; Focarete, M.L.; Gualandi, C.; Arbizzani, C. In Situ Polymerized Poly(1,3-Dioxolane) in Polyacrylonitrile Porous Scaffolds: A Novel Composite Polymer Electrolyte for Room Temperature Battery Application. *J. Power Sources Adv.* **2024**, *26*, 100140. [CrossRef]
48. Wang, Z.-M.; Wang, D.; Dai, W.-K.; Jin, K.-R.; Yang, J.-Z.; Wang, Z.-D.; Tian, Z.-Y. Thermal Decomposition Study of 1,3-Dioxolane as a Representative of Battery Solvent. *J. Anal. Appl. Pyrolysis* **2024**, *182*, 106661. [CrossRef]
49. Melchiorre, M.; Teoh, K.S.; Gómez Urbano, J.L.; Ruffo, F.; Balducci, A. A Lactic Acid Dioxolane as a Bio-Based Solvent for Lithium-Ion Batteries: Physicochemical and Electrochemical Investigations of Lithium Imide-Based Electrolytes. *Green Chem.* **2025**, *27*, 5040–5050. [CrossRef]
50. Information Brochure, Intermediates—1,3-Dioxolane 2013. Available online: http://www.basf.com/performance-materials (accessed on 7 July 2025).
51. Amran, M.; Fediuk, R.; Murali, G.; Vatin, N.; Karelina, M.; Ozbakkaloglu, T.; Krishna, R.S.; Sahoo, A.K.; Das, S.K.; Mishra, J. Rice Husk Ash-Based Concrete Composites: A Critical Review of Their Properties and Applications. *Crystals* **2021**, *11*, 168. [CrossRef]
52. Asutkar, P.; Shinde, S.B.; Patel, R. Study on the Behaviour of Rubber Aggregates Concrete Beams Using Analytical Approach. *Eng. Sci. Technol. Int. J.* **2017**, *20*, 151–159. [CrossRef]
53. Zamora-Castro, S.A.; Salgado-Estrada, R.; Sandoval-Herazo, L.C.; Melendez-Armenta, R.A.; Manzano-Huerta, E.; Yelmi-Carrillo, E.; Herrera-May, A.L. Sustainable Development of Concrete through Aggregates and Innovative Materials: A Review. *Appl. Sci.* **2021**, *11*, 629. [CrossRef]
54. Cota, F.P.; Melo, C.C.D.; Panzera, T.H.; Araújo, A.G.; Borges, P.H.R.; Scarpa, F. Mechanical Properties and ASR Evaluation of Concrete Tiles with Waste Glass Aggregate. *Sustain. Cities Soc.* **2015**, *16*, 49–56. [CrossRef]
55. Choi, Y.-W.; Moon, D.-J.; Chung, J.-S.; Cho, S.-K. Effects of Waste PET Bottles Aggregate on the Properties of Concrete. *Cem. Concr. Res.* **2005**, *35*, 776–781. [CrossRef]
56. Coviello, C.G.; Sabbà, M.F.; Foti, D. Recycled Waste PET for Sustainable Cementitious Materials. In *Comprehensive Green Materials*; Elsevier: Amsterdam, The Netherlands, 2025; pp. 232–260. ISBN 978-0-443-15739-4.

57. Bahmani, H.; Mostofinejad, D. Comparative Analysis of Environmental, Social, and Mechanical Aspects of High-Performance Concrete with Calcium Oxide-Activated Slag Reinforced with Basalt, and Recycled PET Fibers. *Case Stud. Constr. Mater.* **2024**, *20*, e02895. [CrossRef]
58. Bahmani, H.; Mostofinejad, D.; Eftekhar, M.R. A Novel Eco-Friendly Thermal-Insulating High-Performance Geopolymer Concrete Containing Calcium Oxide-Activated Materials with Waste Tire and Waste Polyethylene Terephthalate. *Dev. Built Environ.* **2024**, *18*, 100473. [CrossRef]
59. Dawood, A.O.; AL-Khazraji, H.; Falih, R.S. Physical and Mechanical Properties of Concrete Containing PET Wastes as a Partial Replacement for Fine Aggregates. *Case Stud. Constr. Mater.* **2021**, *14*, e00482. [CrossRef]
60. Tustin, G.C.; Pell, T.M., Jr.; Jenkins, D.A.; Jernigan, M.T. Process for the Recovery of Terephthalic Acid and Ethylene Glycol from Poly(Ethylene Terephthalate). U.S. Patent 5,413,681, 9 May 1995.
61. Porębski, T.; Ratajczak, W.; Tomzik, S.; Kokosiński, W.; Sieradzki, S.; Moderacki, R.; Marton, G.; Krysztofik, P.; Sęp, M.K.; Talma-Piwowar, M. Sposób przerobu zasolonych wód odpadowych z procesu syntezy tlenku etylenu i glikolu 2004. Patent PL186722B1. Available online: https://patents.google.com/patent/PL186722B1/en?q=(Method+of+processing+glycol-containing+saline+waste+waters+por%C4%99bski)&oq=Method+of+processing+glycol-containing+saline+waste+waters+por%C4%99bski (accessed on 7 July 2025).
62. Alfonsetti, R.; De Simone, G.; Lozzi, L.; Passacantando, M.; Picozzi, P.; Santucci, S. SiO_x Surface Stoichiometry by XPS: A Comparison of Various Methods. *Surf. Interface Anal.* **1994**, *22*, 89–92. [CrossRef]
63. Gierada, M. Use of the Cr/SiO_2 Catalysts and Structure of Their Surface Species Zastosowanie Oraz Struktura Form Powierzchniowych Układów Katalitycznych Cr/SiO_2. *Chem. Rev.* **2015**, *1*, 74–79. [CrossRef]
64. Askar, M.K.; Al-Kamaki, Y.S.S.; Hassan, A. Utilizing Polyethylene Terephthalate PET in Concrete: A Review. *Polymers* **2023**, *15*, 3320. [CrossRef] [PubMed]
65. Meza, A.; Pujadas, P.; Meza, L.M.; Pardo-Bosch, F.; López-Carreño, R.D. Mechanical Optimization of Concrete with Recycled PET Fibres Based on a Statistical-Experimental Study. *Materials* **2021**, *14*, 240. [CrossRef] [PubMed]
66. Hadj Mostefa, A.; Slimane, M. Study of Concretes Reinforced by Plastic Fibers Based on Local Materials. *JERA* **2019**, *42*, 100–108. [CrossRef]
67. Polozov, M.A.; Zherebtsov, D.A.; Osipov, A.A.; Radzhakumar, K.; Naifert, S.A.; Spiridonova, D.V.; Zaguzin, A.S.; Vinnik, D.A. Structure of 2,3,5,6-Tetraiodo-1,4-Benzenedicarboxylic Acid and Features of the Thermolysis of Iodinated Terephthalic Acids. *J. Struct. Chem.* **2024**, *65*, 1346–1356. [CrossRef]
68. Wu, J.; Chen, J.; Wang, L.; Zhu, H.; Liu, R.; Song, G.; Feng, C.; Li, Y. Brønsted Acid-Catalysed Aerobic Photo-Oxygenation of Benzylic C–H Bonds. *Green Chem.* **2023**, *25*, 940–945. [CrossRef]
69. Javed, S.; Fisse, J.; Vogt, D. Optimization and Kinetic Evaluation for Glycolytic Depolymerization of Post-Consumer PET Waste with Sodium Methoxide. *Polymers* **2023**, *15*, 687. [CrossRef] [PubMed]
70. Enache, A.-C.; Grecu, I.; Samoila, P. Polyethylene Terephthalate (PET) Recycled by Catalytic Glycolysis: A Bridge toward Circular Economy Principles. *Materials* **2024**, *17*, 2991. [CrossRef] [PubMed]

Disclaimer/Publisher's Note: The statements, opinions and data contained in all publications are solely those of the individual author(s) and contributor(s) and not of MDPI and/or the editor(s). MDPI and/or the editor(s) disclaim responsibility for any injury to people or property resulting from any ideas, methods, instructions or products referred to in the content.